nature nanotechnology

LETTERS

PUBLISHED ONLINE: 5 OCTOBER 2014 | DOI: 10.1038/NNANO.2014.209

Electrostatic control of thermoelectricity in molecular junctions

Youngsang Kim[1†], Wonho Jeong[1†], Kyeongtae Kim[1†], Woochul Lee[1] and Pramod Reddy[1,2*]

Molecular junctions hold significant promise for efficient and high-power-output thermoelectric energy conversion[1–3]. Recent experiments have probed the thermoelectric properties of molecular junctions[4–7]. However, electrostatic control of thermoelectric properties via a gate electrode has not been possible due to technical challenges in creating temperature differentials in three-terminal devices. Here, we show that extremely large temperature gradients (exceeding 1×10^9 K m^{-1}) can be established in nanoscale gaps bridged by molecules, while simultaneously controlling their electronic structure via a gate electrode. Using this platform, we study prototypical Au–biphenyl-4,4′-dithiol–Au and Au–fullerene–Au junctions to demonstrate that the Seebeck coefficient and the electrical conductance of molecular junctions can be simultaneously increased by electrostatic control. Moreover, from our studies of fullerene junctions, we show that thermoelectric properties can be significantly enhanced when the dominant transport orbital is located close to the chemical potential (Fermi level) of the electrodes. These results illustrate the intimate relationship between the thermoelectric properties and charge transmission characteristics of molecular junctions and should enable systematic exploration of the recent computational predictions[1–3] that promise extremely efficient thermoelectric energy conversion in molecular junctions.

Charge transport in molecular junctions has been studied extensively in both two-[8–11] and three-terminal configurations[12–15], because such junctions are excellent candidates for testing quantum transport theories[16–18] and hold significant promise in terms of reaching the ultimate limit of device miniaturization[16]. Experimental efforts[4–7] have also demonstrated two-terminal measurements of thermoelectric properties with a view to obtaining insight into the nature of the dominant charge carriers in molecular junctions. Key to obtaining deeper insights and also the optimization of the thermoelectric properties of molecular junctions is the ability to tune their charge transmission characteristics at the chemical potential (E_F), as their thermoelectric properties are controlled by the magnitude and the derivative of the transmission at E_F (refs 19,20). Although recent pioneering work[12–15] has established the feasibility of actively tuning the charge transmission characteristics of molecular junctions by creating three-terminal devices that feature an additional gate electrode, thermoelectric measurements in such three-terminal configurations have not been achieved. This inability is primarily due to the major experimental challenges in establishing temperature differentials across the source and drain electrodes of molecular junctions and has severely impeded the ability to test several important theoretical and computational predictions[1–3].

To overcome this barrier we performed extensive thermal modelling to conceive a design (Fig. 1a) that offers sufficient thermal resistance between the source and drain electrodes to establish the desired temperature differentials. Specifically, an electrical heater is integrated in close proximity to a Au nanowire. A thin (~7 nm) Al gate electrode is located beneath the Au nanowire and is electrically isolated from it by a 10-nm-thick silicon nitride (SiN_x) dielectric layer (Supplementary Section 1). Our continuum-level thermal modelling, performed using the finite-element method (COMSOL), suggested that when heat is dissipated in the heater and a nanoscale gap is created in the Au nanowire, a temperature differential can be readily established across the nanogap (solid lines in Fig. 1b, bottom; Supplementary Fig. 2). Based on insights obtained from this modelling, we nanofabricated devices that incorporate all the features described above. A scanning electron microscopy (SEM) image of one such device is presented in Fig. 1c.

Following nanofabrication of the device, an electromigration approach was used to create a subnanometre-sized gap in the nanowire (Fig. 1c, see Methods for details). Subsequently, we supplied a sinusoidally modulated electric current at a frequency f (5 Hz) into the integrated heater. This resulted in temperature oscillations at frequency $2f$ (10 Hz) due to Joule heating. To experimentally confirm the presence of a temperature differential across the nanometre-sized gap, temperature fields were characterized using ultrahigh-vacuum scanning thermal microscopy (UHV-SThM)[21,22], an experimental tool developed in our laboratory to quantitatively measure temperature fields with nanoscale resolution. The measured amplitude of temperature oscillations in the vicinity of the nanoscale gap at a temperature of 100 K is shown in the inset of Fig. 1b (top) and features a rapid drop in amplitude across the gap. To further characterize the temperature profile, high-spatial-resolution UHV-SThM imaging (~8 nm) was performed in the immediate vicinity of the nanoscale gap. The measured temperature profile normalized to the heater temperature ($\Delta T_{2f}/\Delta T_{2f,\mathrm{heater}}$) is shown in Fig. 1b (bottom). It can be clearly seen that there is indeed an abrupt drop in the amplitude of temperature oscillations across the gap. Specifically, our detailed experimental thermal characterization (Supplementary Fig. 3) confirms that if the amplitude of the temperature oscillations of the heater is $\Delta T_{2f,\mathrm{heater}}$, then the drop in amplitude across the nanoscale gap ($\Delta T_{2f,\mathrm{Junc}}$) is $(0.34 \pm 0.03) \times \Delta T_{2f,\mathrm{heater}}$ and is in good agreement with the modelling.

Following successful characterization of the temperature fields we used devices identical to those shown in Fig. 1 (that is, electromigrated break junctions with integrated heater) to study the thermoelectric properties of molecular junctions. To accomplish this, we exposed these devices to a solution containing prototypical molecules of biphenyl-4,4′-dithiol (BPDT) or fullerene (C_{60}) (Fig. 1a). This choice was governed by the expectation, from past studies[23–26], that junctions created from BPDT and C_{60} feature off-resonant and resonant charge transport characteristics, respectively. Subsequently, the devices were placed in a cryostat at 100 K (in vacuum) and the electromigration process was initiated (see Methods). This enabled us to stochastically trap (in a subset of

[1]Department of Mechanical Engineering, University of Michigan, Ann Arbor, Michigan 48109, USA, [2]Department of Materials Science and Engineering, University of Michigan, Ann Arbor, Michigan 48109, USA; †These authors contributed equally to this paper. *e-mail: pramodr@umich.edu

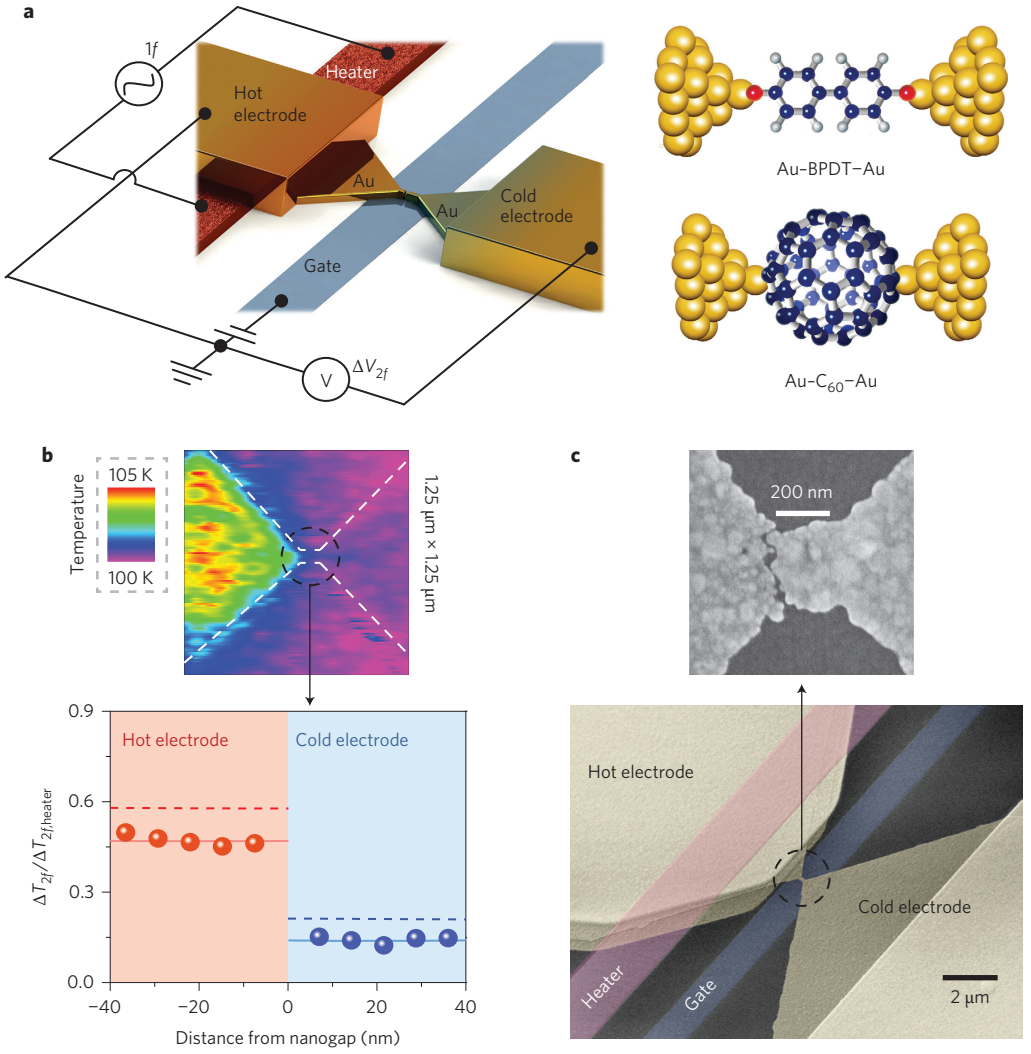

Figure 1 | Experimental platform for tuning the thermoelectric properties of molecular junctions. a, Schematic of the electromigrated break junctions with integrated heater (left) and the molecular junctions studied in this work (right). The temperature differentials across molecular junctions were established using the integrated heater by applying a sinusoidal electric current at frequency 1*f*. The electronic structure of the molecular junctions was tuned electrostatically via the gate electrode. The thermoelectric voltage output (ΔV_{2f}), at frequency 2*f*, was measured by monitoring the voltage differentials between the hot and cold electrodes. **b**, Top: thermal map of a nanogap junction obtained using SThM at 100 K. Dashed lines: outline of the sample. Bottom: normalized temperature profile in the vicinity of the nanogap junction measured using SThM (circles) and calculated by thermal modelling (dotted line). Red and blue solid lines are fits to the measured temperature data on the hot and cold electrodes, respectively. **c**, Bottom: False-coloured SEM image of an as-fabricated device. Top: Magnified SEM image of a nanogap junction formed after electromigration.

devices) one or a few molecules between the electrodes[12–14] (Supplementary Section 4). On trapping the molecules, the gate voltage (V_G)-dependent low-bias conductance G and thermoelectric voltage ΔV_{2f} were measured. Inelastic electron tunnelling spectroscopy (IETS) was also performed on the same junction (see Methods and Supplementary Fig. 13).

The measured low-bias conductance of a Au–BPDT–Au junction ($G_{\text{Au–BPDT–Au}}$) as a function of V_G is shown in Fig. 2a. When V_G is varied from −8 V to +8 V, $G_{\text{Au-BPDT-Au}}$ is shown to decrease systematically. To characterize the thermoelectric properties of the Au–BPDT–Au junctions, temperature modulations ($\Delta T_{2f,\text{Junc}}$) of 1, 2, 3 and 4 K were applied across the junction and the resulting voltage output (ΔV_{2f}) measured as a function of V_G (Fig. 2b). The error bars in Fig. 2a,b correspond to the standard deviation of data obtained from ten independent measurements on the same device (Supplementary Section 3). The magnitude of the measured thermoelectric voltages is seen to decrease systematically on increasing V_G. In Fig. 2c, the Seebeck coefficient of the junction ($S_{\text{Au–BPDT–Au}}$) is shown as a function of V_G (see Supplementary Section 3 for details of the estimation of the Seebeck coefficient). It can be seen that the Seebeck coefficient decreases systematically as V_G is increased, demonstrating that the thermoelectric properties of the junction can indeed be tuned electrostatically by ~35%. Furthermore, $S_{\text{Au–BPDT–Au}}$ is found to be positive for all values of V_G, showing that charge transport is highest occupied molecular orbital (HOMO)-dominated[4,19]. We note that in control experiments performed on pristine electromigrated devices (not exposed to molecules) there was no observable variation in either the low-bias conductance or the Seebeck coefficient of vacuum tunnelling gaps when V_G was varied from −8 V to +8 V. This is consistent with previous studies[27] of the electrical conductance of vacuum gaps in three-terminal configurations (Supplementary Fig. 12), but in strong contrast to the results in Fig. 2, suggesting that the present data correspond to a molecular junction. To further confirm the presence of molecules in the junctions we also performed IETS measurements[13,28,29] and observed vibrational features corresponding to Au–BPDT–Au junctions

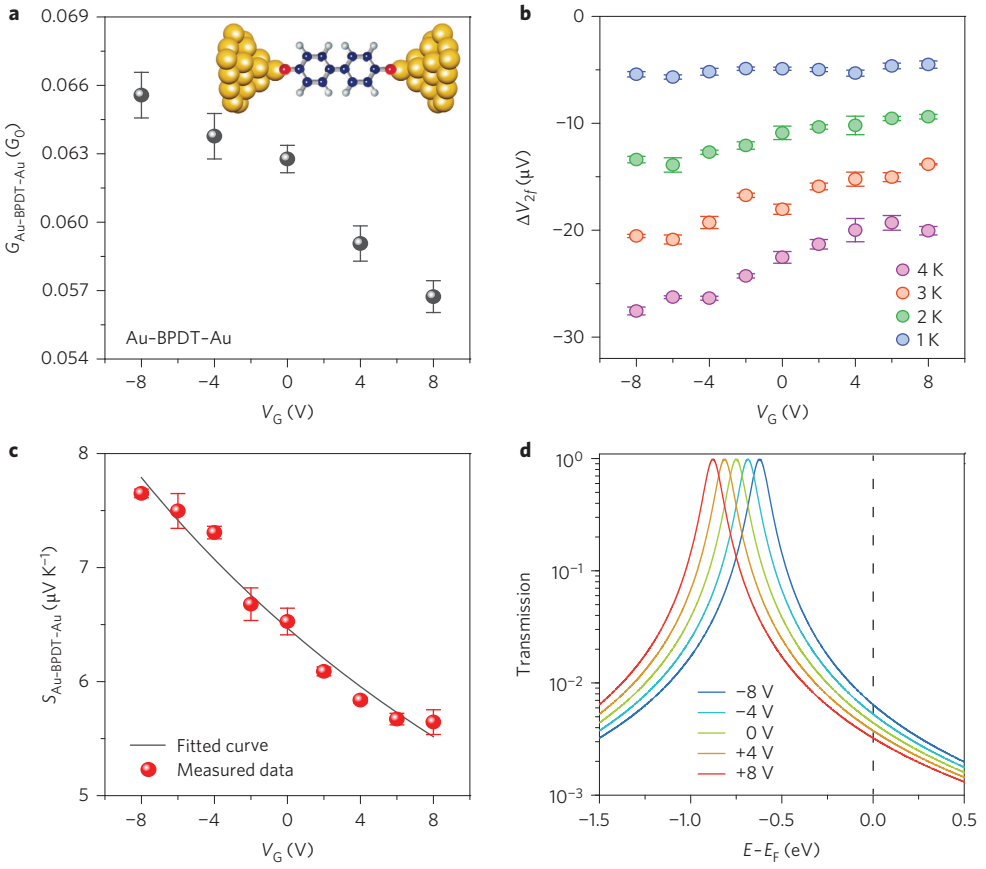

Figure 2 | Effect of tuning the electronic structure on the thermoelectric properties of Au–BPDT–Au junctions. a, Electrical conductance as a function of gate voltage (V_G) for the BPDT junction (see inset). Although the schematic shows a single-molecule junction, the number of molecules in the junction is not necessarily 1. G_0 equals $2e^2/h$, the quantum of electrical conductance. Error bars in **a**–**c** represent the standard deviation of data obtained from ten independent measurements performed on the same device. **b**, Measured thermoelectric voltage output as a function of V_G for various temperature differentials. **c**, Seebeck coefficient of the molecular junction as a function of V_G. The solid line indicates a least-squares fit to the experimental data using equation (2). **d**, Transmission curves as a function of energy for five different values of V_G obtained using equation (1) and the parameters obtained from the least-squares fit. The vertical dotted line indicates the position of the chemical potential, E_F.

(Supplementary Fig. 13). Finally, we note that the data in Fig. 2 are from one of seven Au–BPDT–Au junctions studied (Supplementary Figs 8 and 9 present details of the variability of measurements from different devices).

To obtain a microscopic understanding of the observed dependence of $S_{Au-BPDT-Au}$ on V_G, we adopted a one-level transport model[16,19,28]. Within this model, we assume that the energy- (E) and gate voltage- (V_G) dependent transmission function ($T(E,V_G)$) of a molecular junction is well approximated by a Lorentzian function:

$$T(E,V_G) = \frac{4\Gamma^2}{[E-(E_0-\alpha V_G)]^2+4\Gamma^2} \quad (1)$$

Here, E_0 is the energetic separation of the dominant transport orbital with respect to the chemical potential E_F, Γ represents the coupling of the molecular orbital to the left and right electrodes (assuming symmetric coupling), and α is the effectiveness of gate coupling. From equation (1) it can be shown that the gate voltage-dependent Seebeck coefficient ($S_{Junc}(V_G)$) of the junction is given by[5,7,16,19,20]

$$S_{Junc}(V_G) = -\frac{\pi^2 k_B^2 T_{amb}}{3|e|}\frac{\partial \ln[T(E,V_G)]}{\partial E}\bigg|_{E=E_F} = \frac{\pi^2 k_B^2 T_{amb}}{3|e|}\frac{2[E_F-(E_0-\alpha V_G)]}{[E_F-(E_0-\alpha V_G)]^2+4\Gamma^2} \quad (2)$$

where k_B is the Boltzmann constant, e is the charge of an electron, and T_{amb} is the ambient temperature (100 K in our experiments).

It is clear from equation (2) that a positive Seebeck coefficient implies that $(\partial \ln T(E,V_G)/\partial E)_{E=E_F}$ is negative and that charge transport is HOMO-dominated[4,5,7,19,20,30]. To gain more insight we fit the data in Fig. 2c using equation (2) and a least-squares method to obtain the values of Γ, E_0 and α, which were found to be 0.025 eV, −0.75 eV and 0.016 eV V^{-1}, respectively. Using these values we calculated the transmission functions for various values of V_G from equation (1), which are shown in Fig. 2d. It can be seen that the resonant peak in the transmission shifts by ∼0.26 eV when V_G is swept from −8 V to +8 V, illustrating that the gate electrode is effectively tuning the electronic structure of molecular junctions. It is also clear from Fig. 2d that the peak of the transmission is far from E_F (dotted line) for all values of V_G, showing that transport in Au–BPDT–Au junctions occurs far from resonance. Specifically, the peak of the transmission at $V_G = 0$ V is ∼0.75 eV from E_F and is in good agreement with the results of previous studies[31]. The transmission curves in Fig. 2d can be used to estimate the low-bias conductance of Au–BPDT–Au junctions ($G = G_0 \times T(E = E_F, V_G)$) and is found to decrease monotonically from $\sim 0.006G_0$ to $\sim 0.003G_0$ at E_F when V_G is varied from −8 V to +8 V. These values are smaller than the experimental data in Fig. 2a, suggesting that there are probably multiple molecules in the junction.

In addition to these measurements we also performed corresponding measurements on Au–C_{60}–Au junctions. The measured

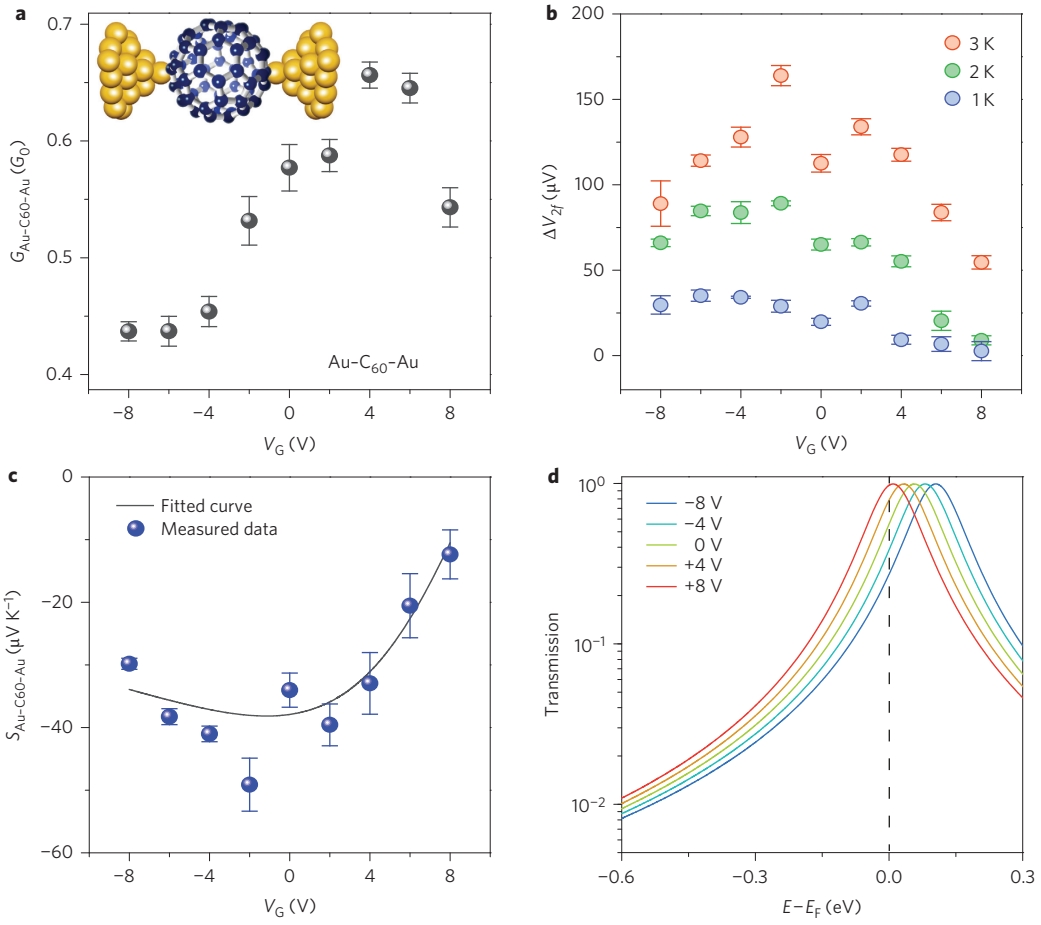

Figure 3 | Effect of tuning the electronic structure on the thermoelectric properties of Au-C_{60}-Au junctions. a–d, As in Fig. 2, but for a Au-C_{60}-Au junction. In contrast to Au-BPDT-Au junctions, charge transport is dominated by the LUMO level (indicated by a negative Seebeck coefficient in **c**). Error bars in **a–c** represent the standard deviation of data obtained from ten independent measurements performed on the same device.

V_G-dependent low-bias conductance, thermoelectric voltage output and Seebeck coefficient ($S_{Au-C60-Au}$) are shown in Fig. 3a, b and c, respectively (the data correspond to one of seven fullerene junctions studied) and the corresponding IETS data are presented in Supplementary Fig. 13. In Au–C_{60}–Au junctions, both the low-bias conductance and the Seebeck coefficient are ~10 times larger than those of Au–BPDT–Au junctions. Furthermore, the Seebeck coefficient can be tuned by a large amount (~300%) by means of electrostatic gating. As shown later, this is primarily due to the resonant charge transport characteristics of C_{60} junctions. It is clear from both the observed increase in low-bias conductance[19] (on increasing V_G) and the negative sign of $S_{Au-C60-Au}$ (refs 6, 32) that charge transport is dominated by the lowest unoccupied molecular orbital (LUMO). Surprisingly, in contrast to Au–BPDT–Au junctions, the measured $S_{Au-C60-Au}$ shown in Fig. 3c neither monotonically increases nor decreases as V_G is increased from −8 V to +8 V. Instead, it exhibits a pronounced minimum and is concaved upwards (U-shaped).

To better understand this behaviour, we again performed a least-squares fit of the Seebeck coefficient data using equation (2) and estimated Γ, E_0 and α to be 0.032 eV, +0.057 eV and 0.006 eV V^{-1}, respectively. The estimated transmission curves for various values of V_G are shown in Fig. 3d and reveal that charge transport in C_{60} junctions is close to resonance (that is, the dominant transport orbital is very close to E_F), a result that confirms previous theoretical predictions[24–26]. The concave-up V_G dependence of the Seebeck coefficient is intimately related to the resonant charge transport properties. Specifically, this dependence arises from a change in the sign of the curvature ($\kappa \propto \partial^2 T/\partial E^2$) of the transmission function at an energy close to the transmission peak, or in other words due to the presence of an inflection point in $T(E,V_G)$. Thus, when V_G is chosen such that the inflection point and E_F overlap with each other, the magnitude of the Seebeck coefficient is maximized. Further changes in V_G move the inflection point away from E_F and result in a decrease in the magnitude of S_{Junc} (Supplementary Fig. 11). We note that the predicted transmission at E_F (Fig. 3d) is consistent with the measured low-bias conductance (Fig. 3a) of the C_{60} junction, suggesting that there is probably only one or a few C_{60} molecules in the junction. Because transport is close to resonance in C_{60} junctions, it is expected that small perturbations in E_0 and/or Γ, which may arise from minor variations in the contact geometry[24–26], could result in a different dependence of $S_{Au-C60-Au}$ on V_G, as is indeed experimentally confirmed (see Supplementary Fig. 9 for additional data sets). Furthermore, the non-monotonic behaviour observed in Fig. 3a at high values of V_G is also possibly due to small reversible variations in the junction geometry introduced by electrostatic perturbations. Finally, we note that the gate coupling of the junctions may be improved by using the principles developed in this work in conjunction with a side-gate scheme that has been demonstrated recently[27].

These results unambiguously demonstrate the direct relationship between the charge transmission characteristics and the thermoelectric properties of molecular junctions. Furthermore, the experimental techniques developed here show that it is indeed possible

to establish large temperature differentials across molecular junctions while actively tuning their thermoelectric properties. This represents a much needed technical advance that provides a rational approach for systematically evaluating intriguing computational predictions[1–3], which suggest that thermoelectric energy conversion can be accomplished (at the Carnot (high efficiency) or Curzon–Ahlborn (high power) limits) in junctions whose charge transmission characteristics are appropriately tuned.

Methods

Electromigration for the creation of molecular junctions. To create the molecular junctions, electromigration was performed following procedures as described elsewhere[13,14,22]. Briefly, electromigrated break junctions with integrated heater (EBJIHs) were mounted in a cryostat after exposure to a solution of the desired molecules (BPDT[13,28] or C_{60}[14]; Supplementary Section 1). Subsequently, electromigration was initiated in vacuum at 100 K by applying a voltage bias across the Au nanowires of the EBJIHs, while continuously monitoring the resistance of the nanowires. The applied voltage was linearly ramped up in steps of 1 mV every 50 ms until the resistance increased by a value that was heuristically chosen to be 1–10% of the nanowire resistance, before initiation of the voltage ramp. On detecting the predetermined increase in resistance, the voltage was rapidly ramped down (~1 ms) to a low voltage (~0.1 V). This process was repeated multiple times until the nanowires broke, forming molecular junctions. The molecular trapping event during electromigration occurs stochastically. In our electromigration experiments, the yield of molecular junctions that demonstrated a non-trivial dependence of both the low-bias conductance and the Seebeck coefficient on V_G was ~3% (14/464) (for more details see Supplementary Section 4).

Thermoelectric voltage measurement. To create temperature differentials across the nanogaps, a sinusoidal electric current was applied to the integrated heater at a frequency of 5 Hz. This resulted in temperature amplitude oscillations at 10 Hz across the molecular junctions. The oscillating temperature differentials resulted in an oscillating thermoelectric voltage output at 10 Hz across the junctions, which was first buffered using a high-input-impedance voltage amplifier (SIM 910) and subsequently measured using a lock-in amplifier (SR 830). The phase information of the thermoelectric voltage output was also recorded to determine the sign of the Seebeck coefficient. In all measurements, V_G was swept in steps of 2 V with a 10 s delay between steps to minimize the effects of capacitive coupling of the gate electrode to other electrodes of the junctions. More details on the determination of the sign of the Seebeck coefficient and quantification of the effect of temperature gradients in the Au thin films of the EBJIHs on the estimated Seebeck coefficient are presented in Supplementary Section 3.

Received 5 May 2014; accepted 21 August 2014; published online 5 October 2014

References

1. Karlström, O., Linke, H., Karlström, G. & Wacker, A. Increasing thermoelectric performance using coherent transport. *Phys. Rev. B* **84,** 113415 (2011).
2. Finch, C. M., García-Suárez, V. M. & Lambert, C. J. Giant thermopower and figure of merit in single-molecule devices. *Phys. Rev. B* **79,** 033405 (2009).
3. Bergfield, J. P., Solis, M. A. & Stafford, C. A. Giant thermoelectric effect from transmission supernodes. *ACS Nano* **4,** 5314–5320 (2010).
4. Reddy, P., Jang, S. Y., Segalman, R. A. & Majumdar, A. Thermoelectricity in molecular junctions. *Science* **315,** 1568–1571 (2007).
5. Widawsky, J. R., Darancet, P., Neaton, J. B. & Venkataraman, L. Simultaneous determination of conductance and thermopower of single molecule junctions. *Nano Lett.* **12,** 354–358 (2012).
6. Evangeli, C. *et al.* Engineering the thermopower of C_{60} molecular junctions. *Nano Lett.* **13,** 2141–2145 (2013).
7. Guo, S. Y., Zhou, G. & Tao, N. J. Single molecule conductance, thermopower, and transition voltage. *Nano Lett.* **13,** 4326–4332 (2013).
8. Lee, W. *et al.* Heat dissipation in atomic-scale junctions. *Nature* **498,** 209–212 (2013).
9. Choi, S. H., Kim, B. & Frisbie, C. D. Electrical resistance of long conjugated molecular wires. *Science* **320,** 1482–1486 (2008).
10. Xu, B. Q. & Tao, N. J. J. Measurement of single-molecule resistance by repeated formation of molecular junctions. *Science* **301,** 1221–1223 (2003).
11. Venkataraman, L., Klare, J. E., Nuckolls, C., Hybertsen, M. S. & Steigerwald, M. L. Dependence of single-molecule junction conductance on molecular conformation. *Nature* **442,** 904–907 (2006).
12. Liang, W. J., Shores, M. P., Bockrath, M., Long, J. R. & Park, H. Kondo resonance in a single-molecule transistor. *Nature* **417,** 725–729 (2002).
13. Song, H. *et al.* Observation of molecular orbital gating. *Nature* **462,** 1039–1043 (2009).
14. Yu, L. H. & Natelson, D. The Kondo effect in C_{60} single-molecule transistors. *Nano Lett.* **4,** 79–83 (2004).
15. Perrin, M. L. *et al.* Large tunable image-charge effects in single-molecule junctions. *Nature Nanotech.* **8,** 282–287 (2013).
16. Cuevas, J. C. & Scheer, E. *Molecular Electronics: An Introduction to Theory and Experiment* (World Scientific, 2010).
17. Bergfield, J. P., Solomon, G. C., Stafford, C. A. & Ratner, M. A. Novel quantum interference effects in transport through molecular radicals. *Nano Lett.* **11,** 2759–2764 (2011).
18. Nitzan, A. & Ratner, M. A. Electron transport in molecular wire junctions. *Science* **300,** 1384–1389 (2003).
19. Paulsson, M. & Datta, S. Thermoelectric effect in molecular electronics. *Phys. Rev. B* **67,** 241403(R) (2003).
20. Ke, S. H., Yang, M., Curtarolo, S. & Baranger, H. U. Thermopower of molecular junctions: an *ab initio* study. *Nano Lett.* **9,** 1011–1014 (2009).
21. Kim, K., Jeong, W., Lee, W. & Reddy, P. Ultra-high vacuum scanning thermal microscopy for nanometer resolution quantitative thermometry. *ACS Nano* **6,** 4248–4257 (2012).
22. Jeong, W., Kim, K., Kim, Y., Lee, W. & Reddy, P. Characterizaion of nanoscale temperature fields during electromigration of nanowires. *Sci. Rep.* **4,** 4975 (2014).
23. Bürkle, M. *et al.* Conduction mechanisms in biphenyl-dithiol single-molecule junctions. *Phys. Rev. B* **85,** 075417 (2012).
24. Bilan, S., Zotti, L. A. & Cuevas, J. C. Theoretical study of the charge transport through C_{60}-based single-molecule junctions. *Phys. Rev. B* **85,** 205403 (2012).
25. Géranton, G., Seiler, C., Bagrets, A., Venkataraman, L. & Evers, F. Transport properties of individual C_{60}-molecules. *J. Chem. Phys.* **139,** 234701 (2013).
26. Ulstrup, S., Frederiksen, T. & Brandbyge, M. Nonequilibrium electron-vibration coupling and conductance fluctuations in a C_{60} junction. *Phys. Rev. B* **86,** 245417 (2012).
27. Xiang, D. *et al.* Three-terminal single-molecule junctions formed by mechanically controllable break junctions with side gating. *Nano Lett.* **13,** 2809–2813 (2013).
28. Kim, Y., Pietsch, T., Erbe, A., Belzig, W. & Scheer, E. Benzenedithiol: a broad-range single-channel molecular conductor. *Nano Lett.* **11,** 3734–3738 (2011).
29. Kim, Y. *et al.* Charge transport in azobenzene-based single-molecule junctions. *Phys. Rev. Lett.* **109,** 226801 (2012).
30. Baheti, K. *et al.* Probing the chemistry of molecular heterojunctions using thermoelectricity. *Nano Lett.* **8,** 715–719 (2008).
31. Tan, A. *et al.* Length dependence of frontier orbital alignment in aromatic molecular junctions. *Appl. Phys. Lett.* **101,** 243107 (2012).
32. Yee, S. K., Malen, J. A., Majumdar, A. & Segalman, R. A. Thermoelectricity in fullerene–metal heterojunctions. *Nano Lett.* **11,** 4089–4094 (2011).

Acknowledgements

P.R. acknowledges support from the Office of Naval Research (award no. N00014-13-1-0320; nanofabrication of devices), the Department of Energy–Basic Energy Sciences (a grant from the Scanning Probe Microscopy Division, award no. DE-SC0004871; scanning thermal microscopy), the Air Force Office of Scientific Research (award no. FA9550-12-1-0058; instrumentation) and the University of Michigan–Ben Gurion University of the Negev Joint Research Collaboration (device modelling). All authors acknowledge the Lurie Nanofabrication Facility (LNF) for facilitating the nanofabrication of devices.

Author contributions

The project was conceived by P.R. Thermopower gating and other electrical measurements were performed by Y.K. and W.J. Nanoscale thermal imaging was performed by K.K. and W.L. Finite-element thermal modelling was performed by W.J. EBJIHs were designed and nanofabricated by W.J., Y.K. and K.K. The manuscript was written by P.R., Y.K. and W.J., with comments and input from all authors.

Additional information

Supplementary information is available in the online version of the paper. Reprints and permissions information is available online at www.nature.com/reprints. Correspondence and requests for materials should be addressed to P.R.

Competing financial interests

The authors declare no competing financial interests.